10-2013

# Co-optimized design of microchannel heat exchangers and thermoelectric generators

A. Rezania
*Aalborg University*

Kazuaki Yazawa
*Birck Nanotechnology Center, Purdue University; University of California - Santa Cruz*, kyazawa@purdue.edu

L. A. Rosendahl
*Aalborg University*

Ali Shakouri
*Birck Nanotechnology Center, Purdue University; University of California - Santa Cruz*, shakouri@purdue.edu



Rezania, A.; Yazawa, Kazuaki; Rosendahl, L. A.; and Shakouri, Ali, "Co-optimized design of microchannel heat exchangers and thermoelectric generators" (2013). *Birck and NCN Publications.* Paper 1472.
http://dx.doi.org/10.1016/j.ijthermalsci.2013.05.002

International Journal of Thermal Sciences 72 (2013) 73–81

Contents lists available at SciVerse ScienceDirect

International Journal of Thermal Sciences

journal homepage: www.elsevier.com/locate/ijts

# Co-optimized design of microchannel heat exchangers and thermoelectric generators

A. Rezania [a,*], K. Yazawa [b,c], L.A. Rosendahl [a], A. Shakouri [b,c]

[a] Department of Energy Technology, Aalborg University, DK-9220 Aalborg, Denmark
[b] Electrical Engineering, Baskin School of Engineering, University of California, Santa Cruz, CA, USA
[c] Birck Nanotechnology Center, Purdue University, IN, USA

ARTICLE INFO

*Article history:*
Received 13 August 2012
Received in revised form
1 May 2013
Accepted 1 May 2013
Available online 13 June 2013

*Keywords:*
Theoretical optimization
Micro plat-fin heat exchanger
Thermoelectric generators
Output power
Cost performance

ABSTRACT

Designs of heat exchangers have mostly been disconnected to the performance of thermoelectric generator (TEG) systems. The development work, mostly focused on thermoelectric materials, required a significant amount of engineering parametric analysis. In this work, a micro plate-fin heat exchanger applied to a TEG is investigated and optimized to maximize the output power and the cost performance of generic TEG systems. The cost per performance is counted by a measure of price per power output ($/W). The channel width, channel height, fin thickness of heat exchanger, and fill factor of TEG are theoretically optimized for a wide range of pumping power. In conjunction with effective numeric tests, the model discusses the optimum size of the system components' dimensions at two area sizes of the substrate plate of heat exchanger. Results show that at every pumping power, there are particular values of channel width and fin thickness that provide maximum output power in the TEG. In addition, for producing maximum cost performance at lower pumping power, larger channel width and channel height and smaller fill factor are required. The results also illustrate that there is a unique pumping power for fixed thickness of fin and ceramic substrates that provides minimum cost per performance for the TEG systems. The theoretical results of the micro heat exchanger are in a good agreement with the experimental investigation data.



## 1. Introduction

Researches in thermoelectric phenomena have mostly focused on developing thermoelectric materials to improve the dimensionless figure-of-merit (ZT) of the material [1,2]. As there is no general model commonly accepted for the whole thermoelectric generator (TEG) system, most of the earlier works required a significant amount of engineering parametric analysis. Although Fukutani et al. [3] optimized thermoelectric refrigerators for integrated circuit cooling applications, there are a few important studies in the case of power generation. Mayer et al. [4] optimized the thickness of the thermoelectric element at which it is thermally matched to the heat exchangers, but this work ignored Peltier and Joule effects in heat transfer. It has been observed that in a model where electrical impedance matching was not considered [5], the maximum power output was achieved when internal thermal resistance matched the sum of external thermal resistances. In addition, in order to obtain the maximum power formula as a function of conversion efficiency, the matching of electrical load, maximum efficiency condition and thermal resistance in a thermal circuit have been considered by Snyder [6,7]. Furthermore, it is shown that the system efficiency at maximum power output is inversely proportional to the sum of heat dissipation in hot and cold thermal resistances [8].

In the power generation systems, a key factor is the optimization of the systems design together with its heat source and heat sink. Effective heat exchanger design is a limiting factor in thermal systems with high heat dissipation rate. To provide high heat flux at the surface of the structure, micro-scale single-phase heat transfer has been widely used in industrial and scientific applications [9]. As is observed, the geometric configuration of the microchannel heat exchanger has a critical effect on the convective heat transfer of laminar flow in the heat exchanger [10,11].

For decreasing the convective resistance at a given substrate area, both the convective heat transfer coefficient and the surface area of the channel walls in contact with the fluid should increase [12]. One way to increase the convective heat transfer coefficient is to reduce the hydraulic diameter of the microchannels. On the

* Corresponding author.
*E-mail address:* alr@et.aau.dk (A. Rezania).

1290-0729/$ – see front matter © 2013 Elsevier Masson SAS. All rights reserved.
http://dx.doi.org/10.1016/j.ijthermalsci.2013.05.002

**Nomenclature**

| | |
|---|---|
| $A$ | area, $m^2$ |
| $b$ | fin thickness, m |
| $C_p$ | specific heat of water, J/kg K |
| $D_h$ | hydraulic diameter of the channel, m |
| $d$ | thermoelement length, m |
| $H$ | channel height, m |
| $h$ | heat transfer coefficient, $W/m^2$ K |
| $F$ | fill factor |
| $K$ | contraction and expansion loss coefficient |
| $k$ | thermal conductivity, W/m K |
| $L$ | heat exchanger length, m |
| $M$ | mass, kg |
| $m$ | resistance ratio, ohm/ohm |
| $\dot{m}$ | mass flow rate, kg/s |
| $N$ | number of elements |
| Nu | Nusselt number |
| $\Delta p$ | pressure drop, Pa |
| $P$ | price, $ |
| Re | Reynolds number |
| $R_{th}$ | thermal resistance, K/W |
| $Z$ | figure-of-merit, 1/K |
| $T$ | temperature, K |
| $t$ | thickness, m |
| $u$ | fluid velocity, m/s |
| $U$ | cost performance, W/$ |
| $W$ | heat exchanger width, m |
| $w$ | power, W |

*Greek symbols*

| | |
|---|---|
| $\delta$ | channel width, m |
| $\eta$ | efficiency |
| $\lambda$ | normalized thickness of substrate |
| $\mu$ | dynamic viscosity, $Ns/m^2$ |
| $\rho$ | density, $kg/m^3$ |
| Ø | spreading angle, deg |

*Subscripts*

| | |
|---|---|
| a | cold reservoir |
| b | base of microchannels |
| ch | channel |
| cr | ceramic substrate |
| hx | heat exchanger |
| f | fluid |
| fin | fin |
| in | inlet |
| max | maximum |
| o | overall |
| out | outlet |
| p | pump |
| pl | plenum |
| s | hot reservoir, substrate plate |
| t | total |
| teg | thermoelement |

other hand, for a given pump power, when the hydraulic diameter decreases, the heat resistance of the heat exchanger increases due to rapid decreasing of the volumetric flow rate. The channel dimensions can be optimized at a practical limit of the available pumping power by minimizing the sum of conductive resistance, convective resistance and heat resistance of the system [13]. At a constant pumping power, when the aspect ratio of the channel becomes larger, the heat transfer area increases, but the volumetric flow rate and fin efficiency decrease. Furthermore, as an important parameter in the output power of the system, the pumping power due to friction factor in the microchannels should be carefully considered.

In order to decrease the coolant pumping power in the TEG system, an effective design of microchannel heat exchanger is proposed and implemented in a three-dimensional TEG model [14]. Nonetheless, when it comes to real-world design of thermoelectric system for direct thermal to electricity conversion, a focused discussion on the TEGs integrated to heat exchangers in micro-scale is still lacking. A consideration of the whole energy conversion system which involves thermal contacts with the hot and cold reservoirs is specifically required. In particular, an analysis of the thermal cost performance, which is a cornerstone for any energy technology, is missing in the thermoelectric field.

In the case of power generation, there are a few important studies [15] that were carried out using optimized analytic models for the parametric analysis of TEG systems. Developing analytic models suitable to predict the performance of micro heat exchangers and TEG can yield a simple approximate approach for designing a TEG system that can achieve maximum power and maximum cost performance. Based on this model, the thermal resistance of the system can be optimized to maximize the cost performance of the system. In addition, the thermal resistance of the microchannel heat exchanger can be minimized for a set of aspect ratio (the ratio of channel height to channel width) [16].

In this study, a TEG system including the system cold side micro plate-fin heat exchanger is optimized parametrically, in order to maximize the output power of the TEG and cost performance of the power system. The cost performance of the system is defined as the difference of output power and pumping power divided by the system mass. This mass includes both the TEG and the heat exchanger. On the other hand, the thermoelectric output power depends on the channel dimensions that define the heat exchanger thermal resistance. Therefore, the modified fill factor and the channel dimensions play key roles in lower material usage and higher output power. The particular focus of this study is exploring the optimum values of these parameters in a wide range of practical pumping power.

This work is based on developing a thermal equivalent network model that takes into account external finite thermal resistances keeping the TEG ceramic substrates and the micro heat exchanger at a fixed temperature difference of hot and cold reservoirs. The Peltier effect and the Joule heating effect are taken into account in the thermal circuit model. The width and height of the microchannels, the fin thickness, and the thermoelements' length that significantly influence power generation are geometrically optimized. The fill factor, which is the fractional area coverage of a thermoelement per unit TEG substrate area, is optimized to generate the maximum system cost performance. In addition, using an effective numeric test, the generated equations also discuss the optimum value of the parameters at two sizes of the heat exchanger substrate plate. Fig. 1a shows the schematic of the TEG system including the heat exchanger. Fig. 1b presents the detailed dimensions of the plate-fin heat exchanger, where water is used as the coolant fluid and the fluid path is made of parallel aluminum

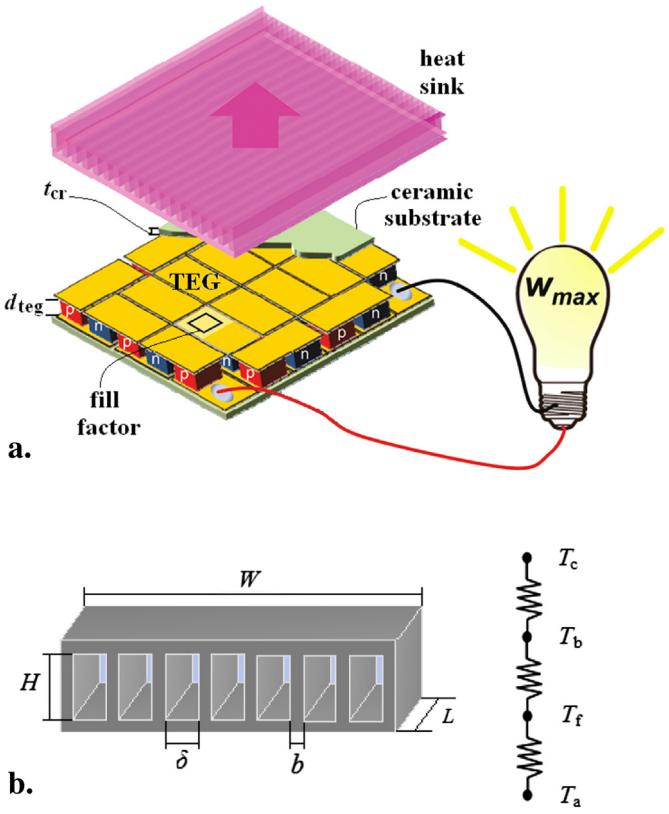


**Fig. 1.** A schematic of the power system. a. TEG system including the heat sink. b. Detailed dimensions of the plate-fin heat sink.

channels. Considering the maturity of industrialization, the cost primarily relies on the price of the raw materials used.

## 2. Model

The output power of a TEG system and its cost performance require the matched thermal resistance design of the sum of thermal resistances of the reservoirs and the ceramic substrates. Thus, the maximum output power and the maximum cost performance must coincide with the minimum external thermal resistances.

### 2.1. Thermal resistance of the micro plate-fin heat exchanger

The channel width, fin thickness and heat exchanger width can define the number of the microchannel. With fixed heat exchanger width, the number of the channel is:

$$N_{ch} = \frac{W}{b+\delta}, \tag{1}$$

where thickness of the heat exchanger side walls is neglected. The thermal resistance of the heat exchanger is independent of the level of dissipated power in forced convection cooling, and is the sum of the conductive resistance due to conduction from the substrate, the convective resistance due to convection from the heat exchanger to the coolant fluid, and the heat resistance due to heating of coolant fluid through the heat exchanger. The flow temperature increases through the microchannels. As the flow absorbs heat, it produces thermal, or heat, resistance. The temperature range of the working fluid, which is water, indicates that Prandtl number is larger than five throughout this study. Thus, it is assumed that a thermally fully developed flow is acceptable [12]. In addition, for a constant heat flux boundary condition, the temperature difference between the heat exchanger base and the bulk coolant fluid is the same at any plane in the flow direction [17]. Therefore, the thermal resistance of the heat exchanger is:

$$R_{th} = \frac{t_{hs}}{k_{hx}A_s} + \frac{1}{\eta_o h_{fin} A_{fin}} + \frac{1}{\dot{m}C_p}, \tag{2}$$

where the first, second and third terms on the right side of the equation are the conductive resistance, convective resistance and heat resistance, respectively. The mass flow rate and the fin area can be defined based on the number of a microchannel as follows:

$$\dot{m} = \rho_f N_{ch} \delta H u, \tag{3}$$

$$A_{fin} = 2N_{ch}(H+\delta)L, \tag{4}$$

and the convective heat transfer coefficient is:

$$h_{fin} = \frac{\mathrm{Nu} k_f}{D_h} \tag{5}$$

Because the aluminum substrate of the heat exchanger has a high thermal conductivity, the conductive resistance is 1% of the convective resistance for $t = 200\,\mu m$ for instance, and can be neglected. For the modeling of the convective resistance, the heat conduction in the fins is assumed to be one dimensional, i.e., only along the fin height, along with constant heat transfer coefficient and uniform fluid temperature. The convective resistance can be divided by a correction factor (fin efficiency) to take into account the thermal resistance of the fins, which implies a non-uniform temperature up the walls. The efficiency for straight rectangular low-thickness fin with an adiabatic tip is defined as follows [18]:

$$\eta_{fin} = \frac{\tanh\left(\sqrt{2h/k_f b}H\right)}{\sqrt{2h/k_f b}H}, \tag{6}$$

Then, the overall surface efficiency of the heat exchanger becomes:

$$\eta_o = 1 - \left(\frac{N_{ch}A_{fin}}{A_t}\right)\left(1-\eta_{fin}\right). \tag{7}$$

Volumetric flow rate in the channels is found simply as the product of velocity and cross-section area. Therefore, the pumping power to circulate the coolant fluid in the heat exchanger is:

$$w_p = N_{ch}\delta H u \Delta p_{ch}, \tag{8}$$

where, in laminar flow regime, the pressure loss throughout the heat exchanger is given by [19]:

$$\Delta p_{ch} = \frac{K\rho_f u^2}{2} + \frac{48\mu L u}{D_h^2}. \tag{9}$$

where $K$ is the contraction and expansion loss coefficient for flow at the heat exchanger entrance and exit, respectively. In this study, the fin thickness is small compared with the channel width; therefore, the first term in (9) can be neglected. By this simplification, the pressure loss relation with the velocity becomes linear. By combining the above equations with (2), the thermal resistance of the heat exchanger is found as:

$$R_{th-hx} = \frac{2\sqrt{3}(b+\delta)}{C_p \rho_f W \delta H \sqrt{\frac{w_p H \delta (b+\delta)}{\mu W L (H+\delta)^2}}} + \frac{H\delta(b+\delta)}{\left(1 - \frac{2LH\left(1 - \frac{\sqrt{2}\tanh\left(\sqrt{\frac{N_{ch}k_f H(H+\delta)(2L+2b)}{H\delta L b k_{hs}}}H\right)}{\sqrt{\frac{N_{ch}k_f H(H+\delta)(2L+2b)}{H\delta L b k_{hs}}}H}\right)}{2LH + L\delta}\right) N_{ch}k_f WL(H+\delta)^2} \quad (10)$$

The range of pumping power for optimizing the considered parameters is from $10^{-3}$ W to 25 W.

### 2.2. Thermal resistance of the ceramic substrates

Typically, thermoelement legs do not occupy the whole foot print of the substrate. Since a small fraction of fill factor reduces the heat flow cross-section area, the spreading thermal resistance should be taken into account. In this study, a model developed by Vermeersch et al. [20] is used to predict the thermal resistance in the ceramic substrates as follows:

$$R_{th-cr} = \frac{\lambda}{k_{cr}(1 + 2\lambda\tan\varnothing)\sqrt{A_{teg}}}, \quad (11)$$

where,

$$\begin{aligned} \varnothing &= 5.86\ln(\lambda) + 40.4 \qquad 0.0011 < \lambda < 1 \\ \varnothing &= 46.45 - 6.048\lambda^{-0.969} \qquad \lambda \geq 1, \end{aligned} \quad (12)$$

and,

$$\lambda = \frac{t_{cr}}{\sqrt{A_{teg}}}. \quad (13)$$

In addition, the footprint area of the thermoelements in this study is defined as follows:

$$A_{teg} = \frac{FWL}{N_{teg}}, \quad (14)$$

where $F$ is the fill factor. Therefore, the thermal resistance of the ceramic substrate is a function of the heat exchanger and the thermoelements as follows:

$$R_{th-cr} = f(t_{cr}, N_{teg}, F, W, L, k_{cr}) \quad (15)$$

This model, which is proposed for the dynamic thermal characterization of a square heat source on a rear cooled substrate, is fitted to exact calculation results for a normalized thickness $\lambda$ ranging from 0.1 to 10. The error of approximation is $\leq$5%.

### 2.3. Output power

According to the analysis of several TEG systems including the heat exchanger, maximum output power occurs when the temperature difference between the hot/cold sides of the TEG legs is approximately equal to one-half of the total temperature difference between the hot and cold flows in the system [21]. In this study, to generate the maximum output power, the thermal resistances of the hot side ceramic substrate and hot reservoirs are taken equal to the thermal resistances of the cold side ceramic substrate and heat exchanger, respectively. Therefore, the optimum electrical impedance match, which is the ratio of the external load resistance to the internal resistance of the TEG, can be expressed as follows [8]:

$$m = \sqrt{1 + Z\overline{T}} = \sqrt{1 + \frac{(T_s + T_a)}{2}}. \quad (16)$$

In addition, the maximum power output, which depends on symmetric external thermal resistances, is found as follows:

$$w_{max} = \left(\frac{Z}{4(1+m)^2 R_{th}}\right)(T_s - T_a)^2. \quad (17)$$

where $R_{th} = 2R_{th-hx} + (2R_{th-cr}/N_{teg})$, and is introduced as external thermal resistances including heat exchangers and widespread thermal resistances. Furthermore, for $Z\overline{T} = 1$, $m = 1.4$.

The Peltier effect and the Joule heating effect that take place at the junctions of the elements and throughout the conductor, respectively, are considered in Eq. (17). This effect, which is additional heat transport, is created by the electric current flow in the system when an external load is connected to the system. In addition, this equation takes into account the Seebeck effect in the TEG. In order to maximize the output power, the optimum leg length of the thermoelement is given as:

$$d = k_{teg} N_{teg} A_{teg} m R_{th}. \quad (18)$$

The optimum dimensions of the microchannels and the TEG are achieved at two substrate sizes ($A_{cr}$ = 2 cm × 2 cm and 4 cm × 4 cm). In addition, the number of thermoelements and the thickness of ceramic substrate are fixed at 400 and 100 μm, respectively. Table 1 shows the variation in fill factor with the selected thermoelement width.

### 2.4. Cost performance

The prices of the key materials in the TEG system are assumed to be 20 $/kg, 100 $/kg and 500 $/kg for the aluminum heat exchanger, TEG ceramic substrates and thermoelectric materials,

**Table 1**
The variation of $F$ with the selected $a_{teg}$ and $N_{teg}$ for maximizing $w_{max}$.

| $W \times L$ (cm$^2$) | 2 cm × 2 cm = 4(cm$^2$) | | | 4 cm × 4 cm = 16(cm$^2$) | | |
|---|---|---|---|---|---|---|
| $a_{teg}$ (mm) | 0.1 | 0.3 | 0.5 | 0.2 | 0.6 | 1.0 |
| $F$ | 0.01 | 0.09 | 0.25 | 0.01 | 0.09 | 0.25 |

respectively. The mass of each microchannel depends on the channel width, channel height and fin thickness. In addition, the total mass of the used thermoelectric material and TEG substrates can be defined based on the substrate dimensions. Therefore, the cost performance of the system is defined as:

$$U = \frac{w_{max} - w_p}{P_t}. \tag{19}$$

where,

$$P_t = 20M_{hx} + 100 \times 2 \times M_{cr} + 500M_{teg} = 20\rho_{hx}HWL\left(1 - \frac{\delta}{b+\delta}\right) + 200\rho_{cr}t_{cr}WL + 500\rho_{teg}d_{teg}FWL. \tag{20}$$

The system cost optimization is discussed at three ceramic substrate thicknesses ($t_{cr} = 2\ \mu m$, $10\ \mu m$ and $50\ \mu m$). Larger thickness of substrate creates larger optimum channel dimensions. Therefore, to keep the optimum channel dimensions within the micro-scale range, the maximum imposed ceramic substrate thickness is 50 μm in this study. To show the effect of fin thickness, the maximum cost performance is discussed at three fin thicknesses ($b = 1\ \mu m$, $10\ \mu m$ and $100\ \mu m$). The heat source temperature and the ambient temperature are assumed as 600 K and 300 K, respectively.

Different channel dimensions and fin thicknesses give different Reynolds numbers. Considering variations in channel width, channel height and fin thickness, the Reynolds number in the microchannels varies from 22.3 to 891.8 in the applied range of pumping power. Li et al. [22] reported that transition to the turbulence regime flow began near Re = 1535 in micro-scale channels, which is lower than the Reynolds number predicted by classical theory. Therefore, the range of Reynolds number guarantees that the flow produced in the microchannel is in laminar regime flow throughout this study.

For the laminar and almost thermally fully developed flow, a constant Nusselt number equal to 3.5 is assumed. However, the exact value of the Nusselt number depends on the shape of the cross-sectional area of the channel. The assumed value is about right for the average aspect ratio in this study [23]. Additionally, as Morini [24] stated, the entrance effects on the average Nusselt number can be neglected if the Graetz number is less than 10 ($Gz < 10$) in the microchannels. Due to the variation of Graetz number in this work, $5.94 < Gz < 8.05$, the Nusselt number is assumed to be independent of the channel entrance effect. Water is used as the coolant fluid in the aluminum heat exchanger. The thermal properties of water are taken as constant at 305 K. Table 2 presents the thermal properties of coolant fluid, heat exchanger, ceramic substrates and thermoelectric materials.

**Table 2**
The thermal properties of the coolant fluid, heat sink, ceramic substrates and thermoelectric materials.

| Dimension | ($kg/m^3$) | | | | (J/kg K) |
|---|---|---|---|---|---|
| Parameter | $\rho_f$ | $\rho_{hx}$ | $\rho_{cr}$ | $\rho_{teg}$ | $C_p$ |
| Value | 999 | 2702 | 3900 | 7200 | 4178 |
| Dimension | (W/m K) | | | | ($N\ s/m^2$) |
| Parameter | $k_f$ | $k_{hx}$ | $k_{cr}$ | $k_{teg}$ | $\mu$ |
| Value | 0.62 | 220 | 30 | 1.35 | $769 \times 10^{-6}$ |

## 3. Validation

Validation of the analytic results is considered in this section. The thermal resistance of the heat exchanger is compared experimentally with the thermal resistance of a micro plate-fin heat exchanger built with twenty microchannels. Table 3 shows the geometric details of the heat exchanger. The experimental data is recorded at thermally steady state in the system for four flow rates (0.010, 0.017, 0.025, 0.034, and 0.041 kg/s) in the heat exchanger. The ultrasonic flow sensor for continuous water measurement with accuracy 0.01% is from Burkert. In order to measure the temperature in the heat exchanger, and the water temperature in the inlet and outlet of heat exchanger, T-type thermocouples are used. An appropriate Labview program is used to record the measurement data.

As shown in Fig. 2, the designed inlet and outlet plenums create U-shaped coolant flow paths in the heat exchanger. Although this type of plenum arrangement provides better uniform mass flow distribution compared with the other studied plenum arrangements in the heat exchanger as discussed by Chein and Chen [25], non-uniformity of velocity and temperature distribution in the heat exchanger still persists. In addition, the contraction and expansion loss coefficients are neglected in this work. These two factors together with the uncertainty of the experimental results make difference between the experimental data and theoretical results as shown in Fig. 3. However the results of experimental investigation and theoretical analysis of the heat exchanger are still in a good agreement. Table 4 shows the percent error of the thermal resistance value between the current work and the experimental data.

The thermal resistance of a single channel is also compared with the results of finite volume method and computational fluid dynamic (CFD) solver, FLUENT. Fig. 4 shows variation of thermal resistance with pumping power in a single channel. The fin thickness, channel width, and height are 40 μm, 400 μm and 800 μm, respectively. Percent error between the two calculations is 1.51% and 12.19% in the studied range of thermal resistance.

## 4. Results and discussion

An analysis of the thermoelectricity focusing only on material development is not comprehensive. In fact, a parametric analysis that considers optimization of the entire TEG system could lead to a different conclusion. For instance, at fixed substrate size and pumping power, the maximum cost performance happens at a smaller fill factor, when the number of thermoelement increases. Furthermore, at fixed substrate size and fill factor, more thermoelements develop smaller thermal resistance in case of ceramic substrates, and provide higher cost performance (Eq. 15). Additionally, as shown in Fig. 5, larger substrate area give larger cost performance due to increasing effect of channel length and number of channels on the heat exchanger. However, larger substrate plate results in lower thermal resistance in the heat exchanger. If the fill factor is equal to 1, the modified thermal resistances of the ceramic substrates are just that of the ceramic substrates. Fig. 6 shows the variation of cost performance with pumping power and fill factor in logarithmic scale at fixed dimensions of microchannels and substrate plate. As can be seen in the figure, there are particular fill factors and pumping powers that provide maximum cost performances. This study explores the optimum system components' dimensions for utilizing full scale effects that lead to maximum output power and cost performance. The results also introduce a compact and light heat exchanger design that takes into account interaction between the micro plate-fin heat exchanger and the TEG as a union energy system.

**Table 3**
The geometric details of the microchannel heat sink used for experimental investigation of heat sink thermal resistance.

| Parameter | $H(\mu m)$ | $\delta(\mu m)$ | $b(\mu m)$ | $D_h(\mu m)$ | $L(mm)$ | $W(mm)$ | $L_{pl}(mm)$ | $D_{pl.in/out}(mm)$ |
|---|---|---|---|---|---|---|---|---|
| Dimension | 700 | 1400 | 1400 | 933 | 56.0 | 56.0 | 50.0 | 5.0 |

### 4.1. Maximum output power

Eq. (15) shows that higher fill factor provides higher system output power due to smaller thermal resistance of the ceramic substrates. In addition, since the fill factor and the scaling parameters of the heat exchanger are not correlated in Eq. (17), the optimum channel dimensions do not vary with the fill factor. Furthermore, as can been seen in Fig. 7, at larger substrate area, the maximum output power takes place at larger channel width and fin thickness. The thicker fin improves heat transfer in the heat exchanger by increasing the fin efficiency that decreases the thermal resistance of the heat exchanger. On the other hand, when the channel width increases at constant pumping power, the heat resistance (third term in Eq. (2)) decreases and produces higher output power. Since fin thickness and channel width are correlated in the definition of heat exchanger area, there is an optimum value of these parameters that can produce the maximum power output. In the studied range of microchannel dimensions, larger channel height produces lower thermal resistance in the heat exchanger, which results in higher output power. The average ratio of channel width to fin thickness is $6.5 < \delta/b < 12.3$ at the considered substrate areas and in the studied range of pumping power. Thus, neglecting the contraction and expansion loss coefficients in Eq. (9) is acceptable in this study.

In conjunction with effective numeric tests, the TEG system can be optimized for various dimensional parameters. Fig. 8 shows the maximum output power and the variation of cost performance in order to provide the maximum output power at different pumping powers. Expectedly, as the pumping power increases, the output power also increases because the thermal resistance of the heat exchanger decreases. Although higher pumping power provides higher output power, a fundamental limit on cost performance occurs when the pumping power becomes comparable to the output power. Beyond a certain value of pumping power, the cost performance value becomes negative. This happens, for instance, at a pumping power equal to 5.35 W for a 2 cm × 2 cm area size of substrate plate.

The thermoelement length is optimized for three fill factors and two area sizes of the substrate plate. In this study, in order to produce a fixed fill factor at different substrate sizes, the footprint area of the thermoelements is changed. A larger substrate size requires a larger optimum thermoelement footprint. Fig. 9 shows the variation of optimum thermoelement length with pumping power variation at different fill factors and substrate areas. As mentioned earlier, higher fill factor produces smaller thermal resistance in the ceramic substrate at constant substrate area. On the other hand, the footprint of the thermoelement increases proportionally with the fill factor. According to Eq. (10), the optimum thermoelement length increases with the fill factor. At constant fill factor and pumping power, as the substrate size of the heat exchanger increases, the thermal resistance of the heat exchanger decreases due to larger effective surface in the heat exchanger. Moreover, the footprint of the thermoelement increases proportionally with the fill factor. Therefore, larger substrate size makes higher thermoelements.

### 4.2. Maximum cost performance

As the model of system cost performance considers the mass of the components in the system, the maximum cost performance does not occur at the maximum output power for a fixed pumping power. In this model, channel height and fin thickness are effective factors in making a light and compact heat exchanger while smaller fin thickness leads to higher cost performance. There is an optimum value for channel height that maximizes the cost performance at any pumping power. As shown in Fig. 10, optimum channel height increases with the ceramic substrate thickness. In contrast with the thicker ceramic substrate, larger channel height produces lower thermal resistance in the heat exchanger, which increases the output power. Therefore, there is a particular value of channel

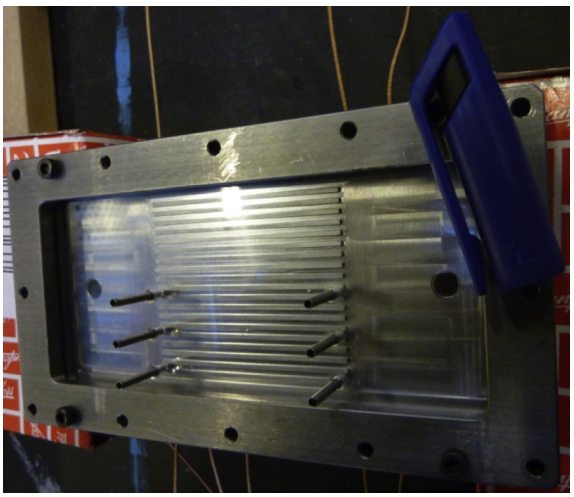

**Fig. 2.** The microchannel heat sink used for experimental investigation of heat sink thermal resistance.

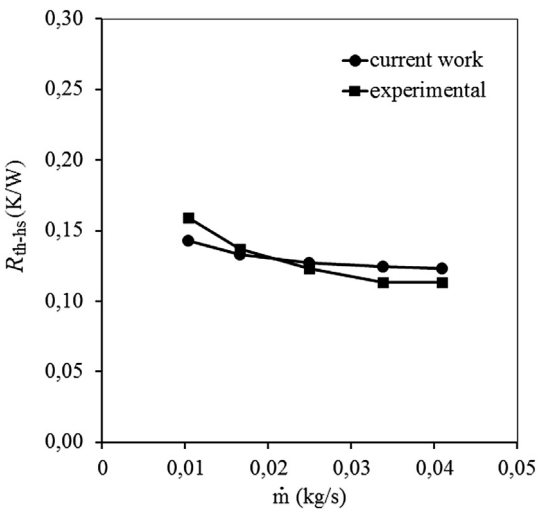


**Fig. 3.** The thermal resistance of the microchannel heat sink compared with the experimental results.

**Table 4**
The percent error of the thermal resistance value between the current work and the experimental data.

| Mass flow rate, $\dot{m}$(kg/s) | 0.010 | 0.017 | 0.025 | 0.034 | 0.041 |
|---|---|---|---|---|---|
| Error, $\left\|\frac{\dot{m}_{EXP}-\dot{m}_{current\ work}}{\dot{m}_{EXP}}\right\| \times 100\%$ | 10.49% | 3.20% | 3.42% | 9.85% | 8.75% |

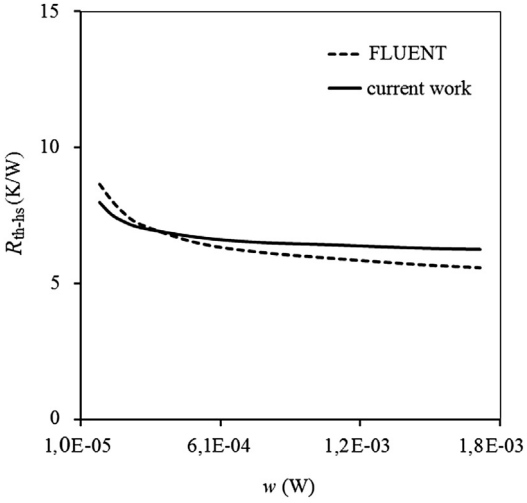


**Fig. 4.** The thermal resistance of microchannel heat sink compared with the results of computational fluid dynamic solver (FLUENT).

height that maximizes the ratio of output power to mass of heat exchanger. In addition, because larger fin thickness increases the overall fin efficiency in the heat exchanger, it requires smaller optimum channel height.

The pumping power due to pressure drop in the microchannels is an important factor for maximizing the cost performance. The number of microchannels affects the mass flow rate distribution in the heat exchanger. The optimum hydraulic diameter of the microchannel can produce minimum pumping power while the thermal resistance of the heat exchanger is minimum. The thickness of the ceramic substrate and the fin thickness also affect the optimum channel width. The optimum channel width, which is

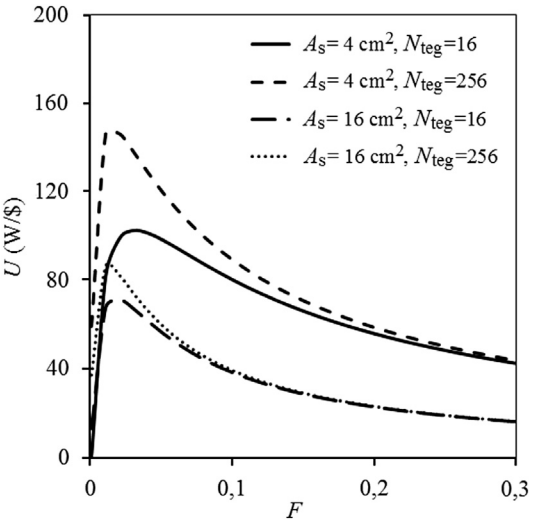


**Fig. 5.** The variation of cost performance with fill factor. $\delta$ = 70 μm, $H$ = 100 μm, $b$ = 10 μm, $w_p$ = 1 W.

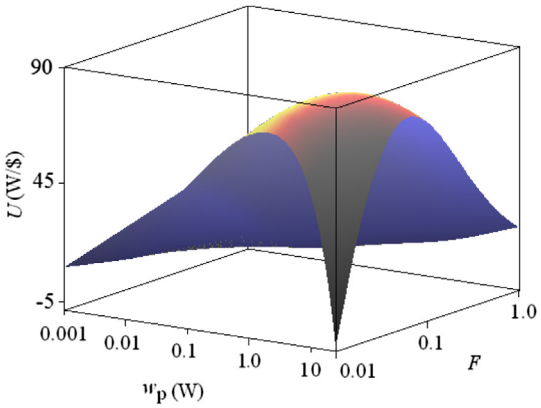


**Fig. 6.** The variation of cost performance with pumping power and fill factor in logarithmic scale, $\delta$ = 70 μm, $H$ = 100 μm, $b$ = 10 μm, $d_s$ = 100 μm.

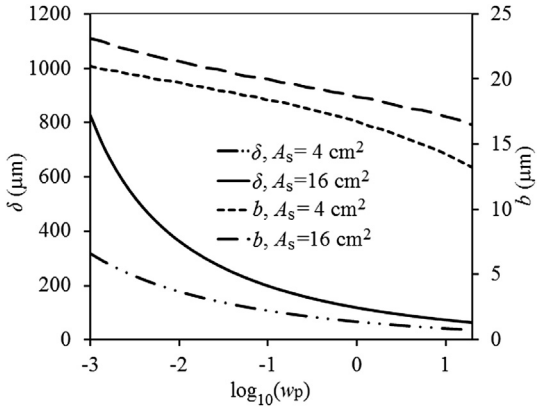


**Fig. 7.** The optimum channel width and fin thickness with the variation of pumping power in order to produce maximum output power, $H$ = 500 μm, $d_s$ = 100 μm.

correlated with the channel height in defining the channel hydraulic diameter, decreases at the thicker ceramic substrate and at the thinner fin, as shown in Fig. 11. In addition, the optimum values of the channel width and the channel height decrease when the pumping power increases.

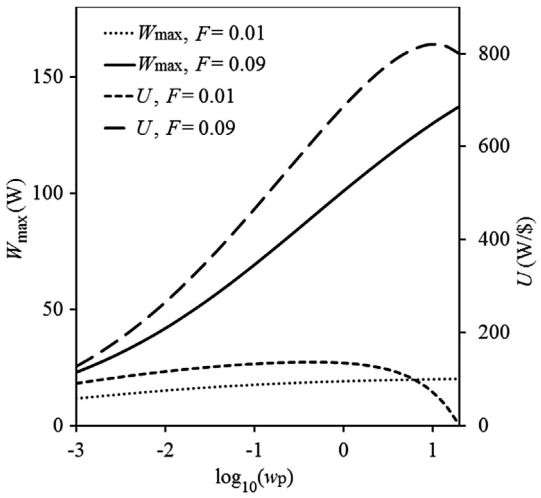


**Fig. 8.** The cost performance and maximum output power of the system with the variation of pumping power, $A_s$ = 4 cm × 4 cm, $H$ = 500 μm, $d_s$ = 100 μm.

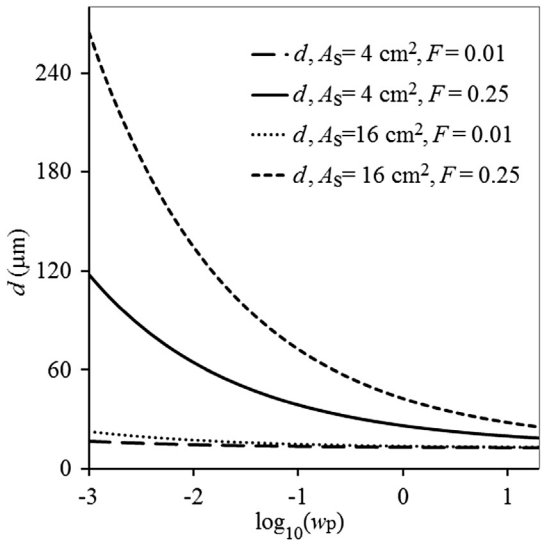


**Fig. 9.** The variation of optimum thermoelement length with pumping power, $H = 500\ \mu m$, $d_s = 100\ \mu m$.

As shown in Fig. 12, in order to maximize the cost performance of the studied power system, a larger fill factor is required as the ceramic substrate thickness increases. The thermal resistance of the ceramic substrate increases with its thickness. One way to decrease the thermal resistance due to ceramic substrate thickness is to increase the fill factor. On the other hand, the mass of the system increases proportionally with the fill factor. Altogether, a thicker ceramic substrate needs a larger fill factor in order to produce the maximum cost performance. The optimum fill factor increases with the pumping power.

Fig. 13 illustrates that there are optimum values of channel width, fin thickness and fill factor that produces the maximum cost performance in the system at every pumping power. As the thickness of both the fin and the ceramic substrate increases, the system thermal resistance as well as the system mass increase while the maximum cost performance decreases. This maximum value occurs at lower pumping power as the thickness of the fin and the ceramic substrate increases. This kind of dependency is shown by Hendricks

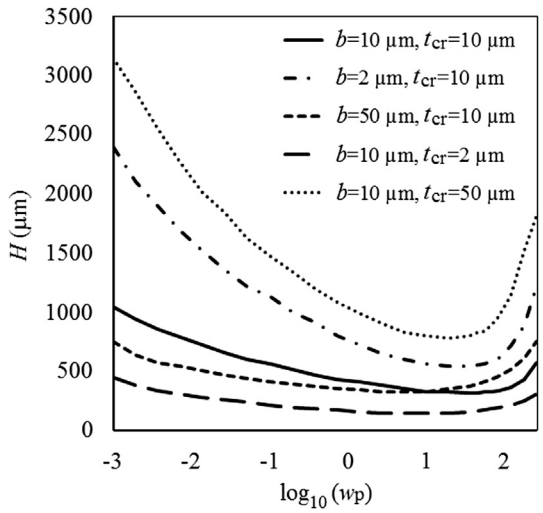


**Fig. 10.** The optimum channel height with the variation of pumping power at three thicknesses of fin and substrate plate, $A_s = 4\ cm^2$.

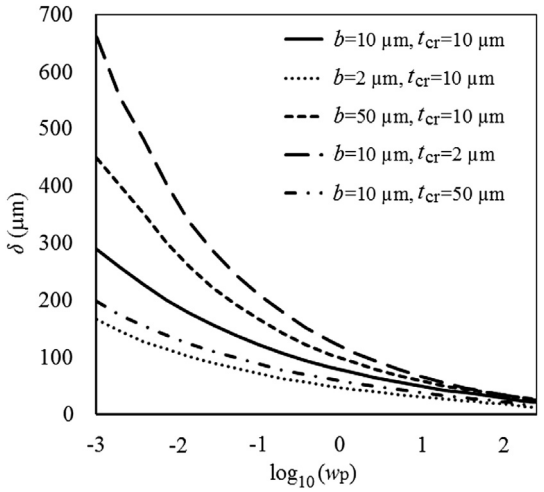


**Fig. 11.** The optimum channel width with the variation of pumping power at three thicknesses of fin and substrate plate, $A_s = 4\ cm^2$.

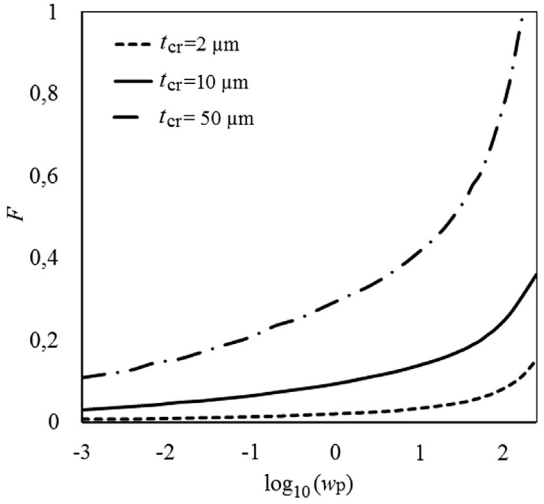


**Fig. 12.** The optimum fill factor with the variation of pumping power at three thicknesses of substrate plate $b = 10\ \mu m$, $A_s = 4\ cm^2$.

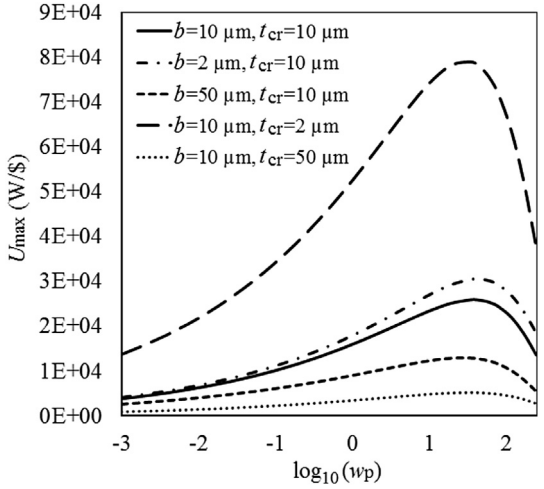


**Fig. 13.** The pumping power and maximum cost performance width variation of pumping power at three thicknesses of fin and substrate plate, $A_s = 4\ cm^2$.

[26] where the dependency of both the heat exchanger's overall heat transfer on the microchannel design specifics is studied for a wide range of pumping power. As mentioned earlier, although the output power of the TEG increases with the pumping power, these two parameters become comparable to each other after a particular pumping power so that the maximum cost performance decreases. The maximum cost performance occurs at lower pumping power as the fin thickness increases. For instance, at $b = 2\ \mu m$, $10\ \mu m$ and $50\ \mu m$, the maximum cost performance occurs at $w_P = 43.1$ W, 35.0 W and 31.0 W, respectively. Note that these values of pumping power produce the maximum overall cost performance in the studied range of pumping power compared with the maximum cost performances at each pumping power.

## 5. Conclusions

In order to maximize the output power and cost performance of TEGs, the channel width, channel height and fin thickness of the applied micro plate-fin heat exchanger along with the fill factor of the TEG are optimized for a wide range of pumping power. In this study, the micro plate-fin heat exchanger applied to the TEG is investigated and optimized in order to maximize the output power and the cost performance of generic TEG systems. The model discusses the optimum size of the system components' dimensions at two area sizes of the substrate plate of heat exchanger. For maximizing the output power, results show that a larger substrate plate switches the maximum output power to the larger channel width, fin thickness and optimum thermoelement length. Additionally, at all the pumping powers studied, there is a particular value of channel width, channel height and fin thickness that produces maximum output power in the TEG. The model also considers the thickness variation effect of the fin and the ceramic substrate on optimized microchannel parameters and fill factor. The results illustrate that there is a unique pumping power that provides the maximum cost performance for the TEG systems.

## Acknowledgments

The authors would like to acknowledge the Center for Energy Materials (CEM) that this work is carried in this center in collaboration with Aarhus University, Denmark. This work is funded in part by the Danish Council for Strategic Research, Programme Commission on Energy and Environment, under Grant No 823032.

## References

[1] A. Bulusu, D.G. Walker, Review of electronic transport models for thermoelectric materials, Superlattices and Microstructures 44 (2008) 1–36.
[2] M.S. Dresselhaus, et al., New directions for low-dimensional thermoelectric materials, Advanced Materials 19 (2007) 1043–1053.
[3] K. Fukutani, A. Shakouri, Design of bulk thermoelectric modules for integrated circuit thermal management, IEEE Transactions on Components and Packaging Technologies 29 (2006) 750–757.
[4] P.M. Mayer, R.J. Ram, Optimization of heat sink-limited thermoelectric generators, Nanoscale and Microscale Thermophysical Engineering 10 (2006) 143–155.
[5] J.W. Stevens, Optimum design of small DT thermoelectric generation systems, Energy Conversion and Management 42 (2001) 709–720.
[6] G.J. Snyder, in: D.M. Rowe (Ed.), Thermoelectric Power Generation: Efficiency and Compatibility, Thermoelectrics Handbook Macro to Nano, Taylor & Francis, 2006 (chapter 9).
[7] G.J. Snyder, in: S. Priya, D.J. Inman (Eds.), Thermoelectric Energy Harvesting, Energy Harvesting Technologies, Springer, 2009 (chapter 11).
[8] K. Yazawa, A. Shakouri, Optimization of power and efficiency of thermoelectric devices with asymmetric thermal contacts, Journal of Applied Physics 111 (2012) 024509-1–024509-6.
[9] P. Rosa, T.G. Karayiannis, M.W. Collins, Single-phase heat transfer in microchannels: the importance of scaling effects, Applied Thermal Engineering 29 (2009) 3447–3468.
[10] X.F. Peng, G.P. Peterson, Convective heat transfer and flow friction for water flow in microchannel structures, International Journal of Heat and Mass Transfer 39 (1996) 2599–2608.
[11] D.D. Ganji, A semi-analytical technique for non-linear settling particle equation of motion, Journal of Hydro-environment Research 6 (2012) 323–327.
[12] D.B. Tuckerman, R.F.W. Pease, High-performance heat sinking for VLSI, IEEE Electron Device Letters 2 (1981) 126–129.
[13] T.J. Hendricks, Microtechnology – a key to system miniaturization in advanced energy recovery & conversion systems, in: Proc. ASME 2008, 2nd International Conference on Energy Sustainability, Paper #ES2008-54244, Jacksonville, FL, 2008.
[14] A. Rezania, L.A. Rosendahl, New configurations of micro plate-fin heat sink in order to reduce coolant pumping power, Journal of Electronic Materials 41 (2012) 1298–1304.
[15] K. Yazawa, A. Shakouri, Cost-efficiency trade-off and the design of thermoelectric power generators, Environmental Science & Technology 45 (2011) 7548–7553.
[16] D. Kim, S.J. Kim, Averaging approach for microchannel heat sinks subject to the uniform wall temperature condition, International Journal of Heat and Mass Transfer 49 (2006) 695–706.
[17] S.J. Kim, Methods for thermal optimization of microchannel heat sinks, Heat Transfer Engineering 25 (2004) 37–49.
[18] F.P. Incropera, D.P. DeWitt, Fundamentals of Heat and Mass Transfer, John Wiley and Sons, New York, 1996.
[19] W.M. Kays, M.E. Crawford, B. Weigand, Convective Heat and Mass Transfer, McGraw-Hill Higher Education, Princeton, 2004.
[20] B. Vermeersch, G.D. Mey, A fixed-angle dynamic heat spreading model for (an) isotropic rear-cooled substrates 130 (2008) 121301-1–121301-9.
[21] J. Henderson, Analysis of a heat exchanger-thermoelectric generator system, in: Presented at the 14th Intersociety Energy Conversion Engineering Conference, Boston, Massachusetts, 1979.
[22] H. Li, R. Ewoldt, M.G. Olsen, Turbulent and transitional velocity measurements in a rectangular microchannel using microscopic particle image velocimetry, Experimental Thermal and Fluid Science 29 (2005) 435–446.
[23] W.M. Kays, A.L. London, Compact Heat Exchanger, McGraw-Hill, New York, 1998.
[24] G.L. Morini, Scaling effects for liquid flows in microchannels, Heat Transfer Engineering 27 (2006) 64–73.
[25] R. Chein, J. Chen, Numerical study of the inlet/outlet arrangement effect on microchannel heat sink performance, International Journal of Thermal Sciences 48 (2009) 1627–1638.
[26] T.J. Hendricks, Microchannel & minichannel heat exchangers in advanced energy recovery & conversion systems, in: Proc. ASME 2006, International Mechanical Engineering Congress & Exposition, Paper #IMECE2006-14594, Chicago, IL, 2006.